ANTITUMOR ACTIVITY OF ISOTOPICALLY MODIFIED ZN^{64} DIASPARTATE ON EHRLICH ASCITES CARCINOMA *IN VIVO*

Max Temnik[1,2], Sergey Gurin[2,1], Oleksandr Balakin[1], Roman Byshovets[3], Ihor Yakymenko[4], Oleksandra Lykhova[5 *], Natalia Bezdieniezhnykh[5]

[1]Analytical Chemistry, Vector Vitale LLC, 3363 NE 163rd Street, Suite 708, North Miami Beach, FL 33160, USA

[2] Biophysics, Metallomix Inc., 175 SW 7th Street, Suite 1702, Miami, FL 33130, USA

[3] Department of Internal Medicine, Bogomolets National Medical University, 13, T. Shevchenko Blvd., Kyiv 01601, Ukraine

[4] Department of Pharmacy, Chemistry and Technologies, Ukrainian State University of Science and Technologies, Lazariana St., 2, 49010 Dnipro, Ukraine

[5] R.E. Kavetsky Institute of Experimental Pathology, Oncology, and Radiobiology of the National Academy of Sciences of Ukraine. 45, Vasylkivska Str., Kyiv 03022, Ukraine

* Corresponding author: Oleksandra Lykhova, R.E. Kavetsky Institute of Experimental Pathology, Oncology, and Radiobiology of the National Academy of Sciences of Ukraine. 45, Vasylkivska Str., Kyiv 03022, Ukraine. [Alexxrna123@gmail.com], ORCID 0000-0003-3622-0489

Keywords: breast cancer, Ehrlich ascites carcinoma, stable isotopes, ^{64}Zn, apoptosis, ROS, p53.

Abstract

Background. In malignant transformation, breast epithelial cells not only accumulate more zinc compared with adjacent histologically normal tissues, but this element also undergoes isotopic fractionation, with breast cancer cells containing predominantly the isotopically light ^{64}Zn. Treatment of breast cancer cells with exogenous Zn^{64} diaspartate enriched with the light zinc isotope may lead to excessive intracellular accumulation of zinc in malignant cells and become an effective inducer of apoptosis through various signaling pathways.

Materials and methods. A new experimental compound Zn^{64} diaspartate enriched with the light stable isotope ^{64}Zn to more than 99% was synthesized. The antitumor effect of Zn^{64} diaspartate was evaluated *in vivo* in a mouse breast cancer model - the Ehrlich ascites carcinoma strain. Tumor cell viability was determined using a trypan blue assay. Carcinoma cell death pathways and apoptosis activation mechanisms were analyzed using flow cytometry, immunocytochemistry, and Western blot analysis.

Results. Zn^{64} diaspartate suppresses the growth of Ehrlich carcinoma in a dose-dependent manner and significantly increases the lifespan of experimental animals. Zn^{64} diaspartate induces tumor cell death by activating apoptosis through increased ROS levels, expression of proapoptotic proteins p53, Bax, Parp-1, and disruption of mitochondrial functional activity.

Conclusion. Zn^{64} diaspartate inhibits Ehrlich ascites carcinoma growth in a dose-dependent manner and induces tumor cell death via activation of the intrinsic, mitochondria-mediated ROS/p53-dependent apoptotic pathway.

Introduction

Breast cancer (BC) is the most common type of cancer diagnosed in women and the second leading cause of cancer-related death among women worldwide [1]. It has been shown that BC cells have an increased need for zinc uptake to support their high proliferation rate and enhanced metabolic activity [2]. Such an excess of zinc in malignant cells is utilized to induce and enhance zinc-dependent processes such as metastasis, angiogenesis, and modification of the tumor microenvironment through the regulation of matrix metalloproteinase production and activity [3]. Therefore, disruption of metal homeostasis, particularly zinc, is one of the significant factors in the pathogenesis of BC [4].

In malignant transformation, breast epithelial cells not only accumulate more zinc compared with adjacent histologically normal tissues, but this element also undergoes isotopic fractionation, with BC cells containing predominantly the isotopically light ^{64}Zn [5]. Research suggests that the differences in isotopic composition are associated with the presence in tumor cells of overexpression of cysteine-rich metallothionein [6]. According to the literature, it is zinc

bound to cysteine, histidine, glutamine, and aspartate that constitutes the 10% mobile, reactive pool of intracellular zinc, through which all zinc-dependent processes in the cell take place [7]. At the same time, it has been demonstrated that excessive intracellular accumulation of zinc in malignant cells leads to activation of apoptosis through various signaling pathways [8]. Therefore, treatment of tumor cells with metallothionein overexpression, such as Ehrlich carcinoma, with exogenous Zn^{64} diaspartate enriched with the light zinc isotope may become an effective inducer of apoptosis in malignant cells.

In this study, we investigated the effect of a new experimental compound, zinc diaspartate enriched with the light stable isotope (^{64}Zn) to more than 99% (Zn^{64} diaspartate), on the growth of experimental mouse breast tumors. The antitumor effect of Zn^{64} diaspartate on BC cells and its mechanisms of action were evaluated in vivo using Ehrlich ascites carcinoma. This spontaneous murine mammary adenocarcinoma has molecular and biological characteristics similar to those of human hormone-receptor–positive BC cells [9], which are the most common subtype encountered in clinical practice [10].

This experimental model was deliberately chosen as the object of study because the cells of this tumor are characterized by a high concentration of Zn–metallothionein [11], which may indicate an extremely important role of zinc, and in particular its light isotopes, in maintaining the metabolism, viability, and proliferation of these BC cells. For the purposes of this study, we hypothesized that the Ehrlich ascites carcinoma (EAC) model would be sufficiently sensitive to the cytotoxic effects of Zn^{64} aspartate, previously demonstrated in cells of different histogenesis [12], which would allow an assessment of the potential antitumor activity of the experimental compound and to identify possible mechanisms of its action on BC cells.

Materials and methods

Investigational Compound. Isotopically modified Zn^{64} diaspartate complex chelated with 2 molecules of L-aspartic amino acid, having a molecular formula $C_8H_{12}N_2O_8{}^{64}Zn$ wherein isotopically light ^{64}Zn is enriched to >99%, molar mass is 328.1 g/mol, and the percentage of ^{64}Zn in the chelate complex is 19.85%.

Animals. Experiments were conducted on outbred female mice aged 10 – 12 weeks old, each weighing 22-25 g. Before the experiment, all animals were tested healthy, with natural behavior and activity profiles. All animals were maintained in accordance with the standards set forth in The Guide for Care and Use of Laboratory Animals (ILAR publication, 1996, National Academy Press, 1996). During the experiment, animals were maintained in the vivarium of the Institute of Experimental Pathology, Oncology and Radiobiology of the National Academy of Sciences of Ukraine ("R.E. Kavetsky IEPOR NAS of Ukraine") in plastic cages in a room with a natural light/dark cycle and were provided a standard diet with ad libitum access to food and water. Animal

protocols were approved by the Bioethics Committee at R.E. Kavetsky IEPOR NAS of Ukraine (protocol No. 3 of May 14, 2018). All studies were conducted in compliance with the rules of the European Convention for the Protection of Vertebrate Animals used for Experimental and Other Scientific Purposes "General principles of animal experimentation" approved by the National Congress on bioethics (Kyiv, 2001–2007) and in concordance with Council directive of November 24, 1986 on the approximation of laws, regulations and administrative provisions of the Member States regarding the protection of animals used for experimental and other scientific purposes (86/609/EEC).

Tumor strain. A strain of Ehrlich ascites tumor cells was obtained from the Bank of Cell Lines from Human and Animal Tissues of R.E. Kavetsky IEPOR NAS of Ukraine and maintained in outbred mice (females) was used in the experiment.

***In vivo* analysis of antitumor activity of drugs.** To transplant the strain, the tumor cells derived from the ascites fluid were placed in saline solution (Yuria Pharm, Ukraine) and 0.3×10^6 cells per mouse (0.3 ml of the suspension) were injected into the abdominal cavity of the subject animals. The animals were grouped randomly into 5 groups:

1. Group I received EAC cells + saline solution via intraperitoneal (IP) injection, and was used for control (n=13);
2. group II received EAC cells + Zn^{64} diaspartate via IP injection at a dose of 22.25 mg/kg (n=13);
3. group III received EAC cells + Zn^{64} diaspartate via IP injection at a dose of 11.13 mg/kg (n=13);
4. group IV received EAC cells + Zn^{64} diaspartate via IP injection at a dose of 5.56 mg/kg (n=13);
5. group V received EAC cells + Cisplatin via IP injection at a dose of 1.5 mg/kg (n=9) for an exploratory control for comparison to a metal-based chemotherapy agent.

The investigational compound, Zn^{64} diaspartate, was administered every other day for 12 days, a total of 6 administrations with a cumulative dose of 133.50 mg/kg for Group 2; a cumulative dose of 66.78 mg/kg for Group 3; a cumulative dose of 33.36 mg/kg for Group 4. Cisplatin (Ebewe, Austria) was administered every other day for 6 days, a total of 3 administrations with a cumulative dose of 4.5 mg/kg) [13]. The first injection of Zn^{64} diaspartate and Cisplatin was administered 24 hours after the tumor cell inoculation.

Three animals from each group were euthanized via cerebral dislocation method on the 19^{th} day after intraperitoneal injection of tumor cells (or 6 days after the last injection of Zn^{64} diaspartate). At the same time, ascites fluid was collected from the animals' abdomen by washing their peritoneal cavity with saline solution, and live/dead EAC cells were counted using the trypan blue (HyClon, USA) exclusion test and the Goryaev's chamber (Voles, Ukraine). To determine the presence of EAC cells in the peritoneal cavity of experimental animals, the collected cells were diluted in saline to a concentration of $1x10^6$ and 40 μl of the cell suspensions were transferred onto

a glass slide (Aptaca, Italy) using a cytocentrifuge (Biosan, Latvia). The cells were then air-dried and stored at -20°C. Prior to staining, the specimens were thawed at room temperature and stained using Pappenheim staining method: the specimens were placed in a May-Grünwald (Merck, Germany) staining cuvette continually for 3 minutes. Sequentially, the stain was diluted by adding an equal amount of distilled water, and staining continued for an additional 3 minutes. Sequentially, the specimens were rinsed with an ample amount of distilled water to remove the stain, and air-dried. After dehydration, the specimens were stained in an aqueous solution of diluted Romanovsky (Shostka Chemical Reagents Factory, Ukraine) stain (1:5) for 20 minutes and then rinsed thoroughly with distilled water and air-dried. The stained specimens were examined and imaged using an Axiostar Plus microscope (Carl Zeiss, Germany), equipped with a PowerShot G5 digital camera (Canon, United Kingdom) at x1000 magnification.

The remaining animals from all groups (or 10 mice per group) were used to assess their survival in the experiment. The total observation period for this assessment was 40 days following tumor cell inoculation.

Study of the *in vivo* mechanisms of action of ^{64}Zn diaspartate on the tumor cells.

Transplantation of carcinoma strain. To transplant the strain, the tumor cells derived from the ascites fluid were placed in saline solution (Yuria Pharm, Ukraine), and 5×10^6 cells per mouse (0.3 ml of the suspension) were injected into the abdominal cavity of animals. The animals were allocated randomly into three groups:

1. group I received EAC cells + saline solution intraperitoneal (IP) injection, and used for control (n=9);
2. group II received EAC cells + Zn^{64} diaspartate IP injection at a dose of 22.25 mg/kg (n=9);
3. group III received EAC cells + Zn^{64} diaspartate IP injection at a dose of 11.13 mg/kg (n=9).

A single IP injection of Zn^{64} diaspartate was performed 24 hours after inoculating tumor cells. The animals were euthanized via cerebral dislocation method 24 hours after Zn^{64} diaspartate injections, and all cells were collected from their peritoneal cavities by washing them with saline solution. Live/dead EAC cells collected from each mouse were counted in the obtained suspension using the trypan blue exclusion test and the Goryaev's chamber.

To derive macrophages, all cells collected from the peritoneal cavities of control and experimental animals were transferred to Petri dishes d=10 mm for cell culture (SPL, Korea). 10 ml of DMEM (Biowest, France) complete medium supplemented with 10% FBS (Biowest, France) and 40 μg/ml gentamicin (Sigma, USA) were added to each sample. The cells were incubated in a CO_2 incubator (Heal Force, China) for 2 hours at 37°C in the presence of 5% CO_2. Under such conditions, macrophages adhere to the surface of the Petri dish, while other cells remain in the suspension. As soon as the incubation was complete, cells that did not adhere to the surface of the

Petri dish were collected in test tubes and washed with PBS (Sigma, USA) twice at 1500 rpm for 10 minutes. The obtained cellular precipitate was resuspended in 1 ml of PBS, the number of live/dead cells in each sample was counted using trypan blue and Goryaev's chamber. The resulting cell suspension was used in subsequent studies.

Determination of tumor cell death indices. The numbers of live, apoptotic, and dead cells in the experiment were determined using flow cytometry. The isolated cells were centrifuged at 400g for 7 minutes. The supernatant was then removed, and 0.7 ml of annexin binding buffer (10 mol/L Hepes, 140 mol/L NaCl, 2.5 mol/L $CaCl_2$) (Sigma-Aldrich, USA) was added to the cellular precipitate and then adjusted to a final concentration of 0.6 μg/ml with Annexin-GFP (IBCH, Ukraine). Cells were incubated at room temperature for 30 minutes in the dark. After incubation, propidium iodide (PI) (Sigma-Aldrich, USA) was added to the samples to achieve a final concentration of 10.0 μg/ml, and the cells were incubated at room temperature for an additional 15 minutes. The samples were then analyzed using a COULTER EPICS XL flow cytometer. Fluorescence signals of the test samples were recorded using the FL1 channel (515-535 nm) for GFP and FL3 channel (620-630 nm) for PI. More than 5,000 events from each sample were analyzed. The percentage of live, apoptotic and dead cells was calculated based on the results of staining the cells with fluorescent dyes (PI, Annexin-GFP) in the FCS Express V3 program.

Immunocytochemistry assay (ICC). The isolated cells were diluted with saline to a concentration of $5x10^5$ and 40 μl of the cell suspension was transferred onto glass slides using a cytocentrifuge. Cytospin preparations were then air-dried and stored at -20°C. Before analysis, the preparations were thawed at room temperature and fixed with methanol (Sigma, USA)/acetone (Chimreserve, Ukraine) solution (1:1) for 2 hours at -20°C. They were then washed 3 times with PBS. An ICC reaction was performed using an Ultra Vision Quanto Detection System (Thermo Scientific, USA) according to the manufacturer's instructions. Primary monoclonal antibodies against Bcl-2 100/D5, Bax 6A7, p53 clone Y-5 (Thermo Fisher Scientific, USA) and p53 clone DO-7 (Dako, Denmark) were used. Cells treated with mAbs were incubated at room temperature for 60 minutes. A Poly Vue imaging system conjugated with peroxidase (Thermo Scientific, USA) was then used and enzyme activity was detected using diaminobenzidine as a substrate. When the ICC reaction was completed, the preparations were washed with distilled water and stained with hematoxylin (Thermo Scientific, USA). The results were analyzed by counting cells with marker expression (brown stained cells) using an Axiostar Plus light microscope and evaluated using the classical H-Score method: S = 1xA+2xB+3xC, where S is the H-Score index having the values within a range from 0 (no protein detected) to 300 (intense expression in 100% of cells), A - the percentage of weakly stained cells, B - the percentage of moderately stained cells, C - the percentage of strongly

stained cells. The observation results were fixed using a Canon PowerShot G5 digital camera at x400 magnification.

Western blot analysis. To separate proteins by electrophoresis, samples of cell lysates (in RIPA buffer (Thermo Scientific, USA) supplemented with protease and phosphatase inhibitors) were heated at 95°C for 5 min in Laemmli buffer (Sigma, USA) for the samples. Electrophoresis was performed in Tris-glycine buffer (pH 8.3) (Sigma, USA) using a Mini-PROTEAN II electrophoresis chamber (BIO-RAD, Sweden). Quantitative proteins were separated in a 12% sodium dodecyl sulfate polyacrylamide gel (Sigma, Germany) (SDS-PAG) in the Laemmli buffer system. To determine molecular weights of proteins on electrophoregrams, protein standards covering a molecular weight range of 10-250 kDa were used. Proteins were transferred from polyacrylamide gel (PAG) to a nitrocellulose membrane (Amersham Bioscience, UK) in an electric field, in a Mini Trans-Blot Cell unit (BIO-RAD, Sweden), in transfer buffer containing 2.5 mmol/L Tris-HCl, pH 8.3, 20% methanol (Sigma, USA), 192 mmol/L glycine, 0.1% SDS (Sigma, Germany). The membranes were washed with distilled water and stained for 5-10 min with 1% Ponceau S dye solution (Sigma, USA) prepared in 3% trichloroacetic acid (Sigma, USA). Free binding sites on the membrane were then blocked for 1 h with 5% skim milk (APEX Research, Inc.) in PBS and 0.1% Tween 20 detergent (Sigma, USA). The membranes were incubated with primary antibodies overnight at +4°C, followed by washing with PBS. Primary monoclonal antibodies against NF-kB (Sigma, USA), p53 and p38α/β (Santa Cruz Biotechnology, USA), phospho-p38 and Parp-1 (Cell Signaling Technology, USA) were used. Antibodies against tubulin (Sigma, USA) were used to normalize protein levels in the band intensity analysis (densitometry). Antispecies horseradish peroxidase-conjugated antibodies (Sigma, USA) were used as secondary antibodies. Immunoreactive bands were detected by a solution containing 1.25 mmol/L luminol, 2.72 mmol/L coumaric acid and 0.01% hydrogen peroxide in 0.1 M Tris-HCl (pH 8.5) (Sigma, USA). Exposure time of the treated membranes on X-ray film (Thermo Scientific, USA) depended on the intensity of chemiluminescence reaction. Carestream Kodak reagents (Sigma, USA) were used for X-ray film development. The band intensities were quantified using Total Lab software.

Reactive oxygen species production in tumor cell. ROS production in the carcinoma cells was assessed using flow cytometry. The 0.5×10^6 cells were suspended in 0.5 ml of a 15 μM DCF-DA solution (Sigma-Aldrich, USA) in PBS. Cells were incubated at room temperature for 30 minutes in a dark place. After incubation, cells were washed three times with PBS. The samples were then analyzed using a COULTER EPICS XL flow cytometer. Fluorescence signals of the test samples were recorded using the FL1 channel (515-535 nm). More than 5,000 events from each sample were analyzed. The DCF-DA fluorescence intensity in the cells was measured using the FCS express V3 program.

Assessment of the state of cardiolipin in carcinoma cells. The $1x10^6$ cells was resuspended in PBS and 10-N-nonyl acridine orange (NAO) (Sigma-Aldrich, Germany) dye was added to all samples, except the negative (unstained) control samples, and incubated for 30 min at 37°C and 5% CO_2. After incubation, cells were washed three times with PBS. The samples were then analyzed using a flow cytometer by the shift in fluorescence intensity to the right from an appropriate control.

Statistical analysis. The results are presented as the mean (M), standard deviation (SD) and the standard error of the mean (± m). Statistical data processing was performed using MS Excel and Origin 7.5 software. Differences between the comparison group means were determined by one-way analysis of variance (one-way ANOVA) followed by the Tukey test (post-hoc test). Differences between groups were considered statistically significant at $p < 0.05$.

Results and Discussion

Our hypothesis is that because ^{64}Zn is a light stable isotope enriched to >99% isotopic purity over its 48.6% natural abundance, Zn^{64} diaspartate functions as a metallome-targeting therapeutic rather than a conventional cytotoxic drug, exploiting cancer-associated zinc transporter dysregulation and zinc-dependent enzyme networks in the tumor microenvironment. Furthermore, it is the ^{64}Zn compound, containing aspartic acid, that may be the form with high bioavailability due to the important role of such substances in ensuring cellular homeostasis. So, isotopically modified zinc complexes as a new class of anticancer agents and provide a mechanistic basis and dosing logic for further preclinical and early clinical development.

The antitumor effect of Zn^{64} diaspartate is evidenced by the absence or statistically significant reduction in the volume of ascitic fluid by 90% (vs control group) in the abdominal cavity of mice that received injections of the test compound at doses of 22.25 mg/kg and 11.13 mg/kg, respectively (Figure 1a). The antitumor effects of Zn^{64} diaspartate in the EAC model are also supported by the results of tumor cell viability assessment and microscopic cytomorphological analysis of cells from the peritoneal cavity of mice in the control and experimental groups. According to these indicators on the 19^{th} day after inoculation of EAC cells showed that Zn^{64} diaspartate statistically significant suppressed the growth of EAC tumors compared with the control: a lower number of living tumor cells by 84.8-98% (Figure 1b, Figure 1c). The group of mice that received cisplatin was used as a positive control, since this metal-containing cytostatic agent is employed in the treatment of BC [14]. The animal group treated with cisplatin showed the number of viable cells in the peritoneal cavity 45.9% lower vs control (Figure 1b, Figure 1c).

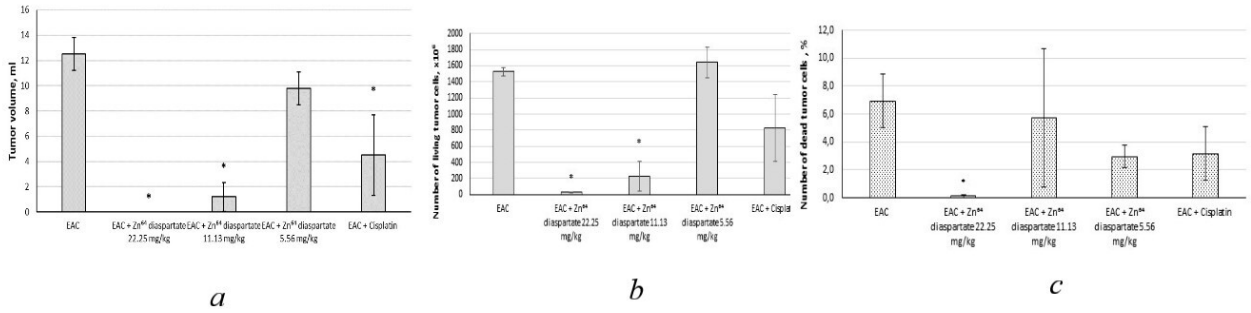


Figure 1. Volume of ascites fluid (*a*) and number of viable (*b*) and dead cells (*c*) in abdominal cavity of mice on the 19th day after EAC transplantation (n=3). *The difference between treated and control groups is statistically significant when $p<0.05$

The microscopic analysis showed that although in most mice treated with Zn^{64} diaspartate dosed 22.25 mg/kg no carcinoma cells were found (Figure 2c), in the abdominal cavity of some animals of this group against a background of a substantial number of macrophages and neutrophils, single malignant cells were observed (Figure 2b). Animal groups that received Zn^{64} diaspartate dosed 11.13 mg/kg and cisplatin observed similar heterogeneous situation, but the number of tumor cells was greater (Figure 2d, e, j, h).

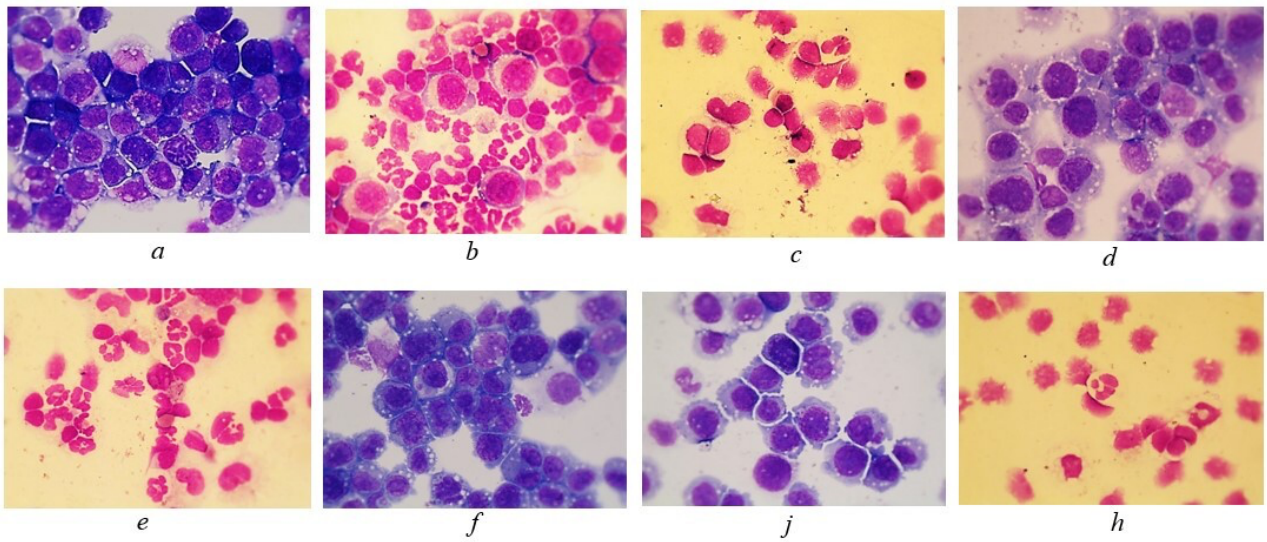


Figure 2. Microscopic analysis of cells collected from peritoneal cavities of experimental animals (n=3). (*a*) – EAC, (*b, c*) - EAC + Zn^{64} diaspartate 22.25 mg/kg, (*d, e*) - EAC + Zn^{64} diaspartate 11.13 mg/kg, (*f*) - EAC + Zn^{64} diaspartate 5.56 mg/kg, (*j, h*) - EAC + cisplatin. The cells were fixed and Pappenheim staining, magnification x1000.

The primary efficacy endpoint for antitumor drugs in ascites tumor models is animal survival. Comparative analysis of Kaplan–Meier curves and the mean survival of mice with EAC in the control and experimental groups demonstrated a substantial and statistically significant

increase in the survival of animals treated with Zn^{64} diaspartate, at a level comparable to cisplatin (Figure 3).

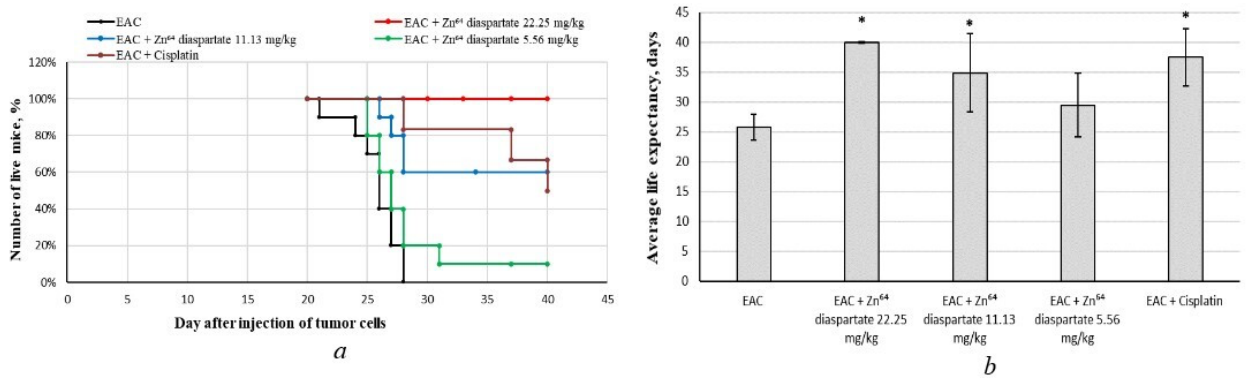


Figure 3. Effects of different Zn^{64} diaspartate doses of on the survival rate of mice with EAC. Observations lasted 40 days from the moment of transplantation of the experimental tumor (n=10). (*a*) Comparison of survival curves (Kaplan-Meier curves) of control and experimental groups of animals. (*b*) Effect of Zn^{64} diaspartate on the average lifespan of mice with EAC. *The difference between treated and control groups is statistically significant when $p<0.05$

The obtained results indicate that Zn^{64} diaspartate statistically significant suppresses the growth of experimental EAC in a clear dose-dependent manner, indicating a pharmacologic effect rather than nonspecific toxicity. The "heterogeneity" of antitumor effect reflects features of the mechanism of action of this compound and therefore do not affect all tumor cell subpopulations in the same way. We hypothesize that Zn^{64} diaspartate perturbs metal-dependent cellular processes [15] in the context of spatial heterogeneity and polyclonal tumor features [16]. This non-overlapping activity profile suggests potential for combination regimens, reduced cross-resistance, and broader applicability across tumors with zinc dysregulation.

To identify possible molecular mechanisms underlying the antitumor action of Zn^{64} diaspartate, we assessed the effects of different doses on EAC cell viability and mode of cell death, as well as on ROS production, mitochondrial status and functional activity, and the expression of apoptosis-regulating proteins. These effects were evaluated *in vivo*, which is more informative than *in vitro* studies because this system preserves the complex interactions of Zn^{64} diaspartate with the organism as a whole, including immune responses, metabolism, blood flow, and drug distribution.

Cell viability in tumor cells from the control and experimental groups was determined using the trypan blue exclusion assay. It was shown that Zn^{64} diaspartate induced statistically significant decrease in the number of viable EAC cells by 52–64% and an increase in the number of dead cells by 2.7- and 6.7-fold relative to the control group (Figure 4 a1, a2).

Importantly, in the peritoneal cavity of mice treated with Zn^{64} diaspartate, there was an accumulation of adhesive cells (Figure 4b), predominantly neutrophils and macrophages [9]. The presence of a greater number of such cells in the peritoneal cavity of animals in the treated animal groups compared to control may indicate activation of nonspecific antitumor immunity, both as a result of EAC cell death under the action of the test substance and due to the direct effect of Zn^{64} diaspartate itself. However, these changes in immune system reactivity in the experimental animals require further studies aimed at a more detailed investigation of the activation of various components of nonspecific and specific antitumor immunity.

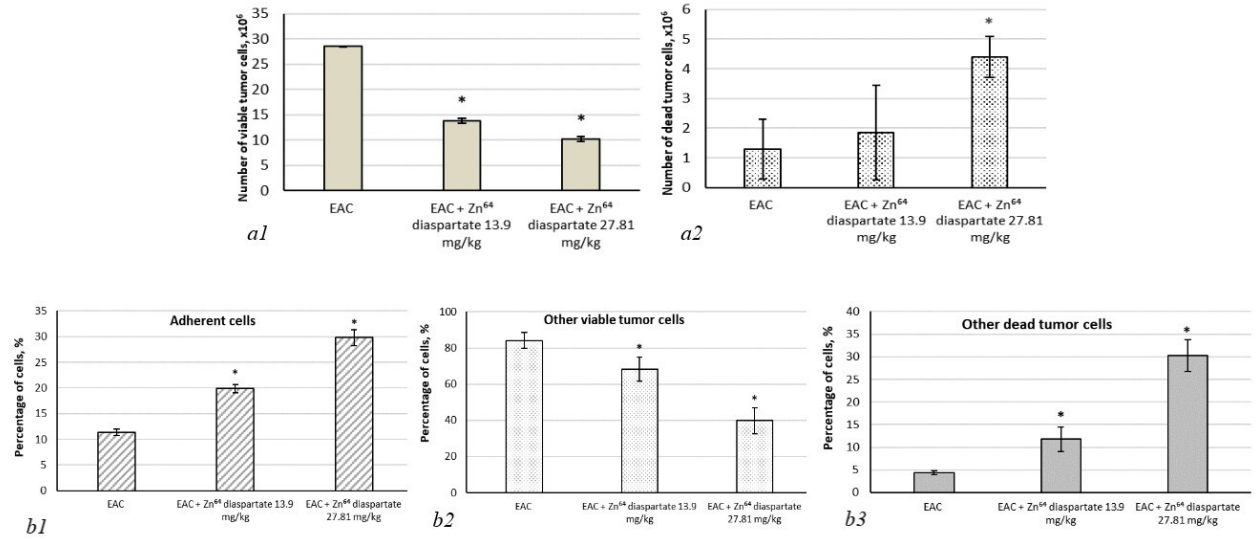


Figure 4. Effects of Zn^{64} diaspartate on viability of EAC cells (*a1, a2*) and percentage of adhesives (*b1*), other viable (*b2*) and dead (*b3*) tumor cells (n=9). The viability of carcinoma cells was determined using the trypan blue test. *The difference between treated and control groups is statistically significant when $p<0.05$

To determine the mechanisms of EAC cell death *in vivo* after administration of Zn^{64} diaspartate, we used Annexin V- GFP/PI cytometric test (Figure 5). It was showed that as early as 24 hours after the first injection of the compound, 30%–45% of tumor cells in the peritoneal cavity of carcinoma-bearing animals died predominantly via apoptosis: increases the number of carcinoma cells in the early/middle and late phases of apoptosis by 3-7 times in Zn^{64} diaspartate treated groups comparative to control ($p<0.05$).

An analysis of the cellular redox system, mitochondrial functional activity, and the expression levels of cell-cycle regulatory proteins and pro- and anti-apoptotic proteins revealed that Zn^{64} diaspartate at the tested doses induced apoptosis in EAC cells in the manner described below.

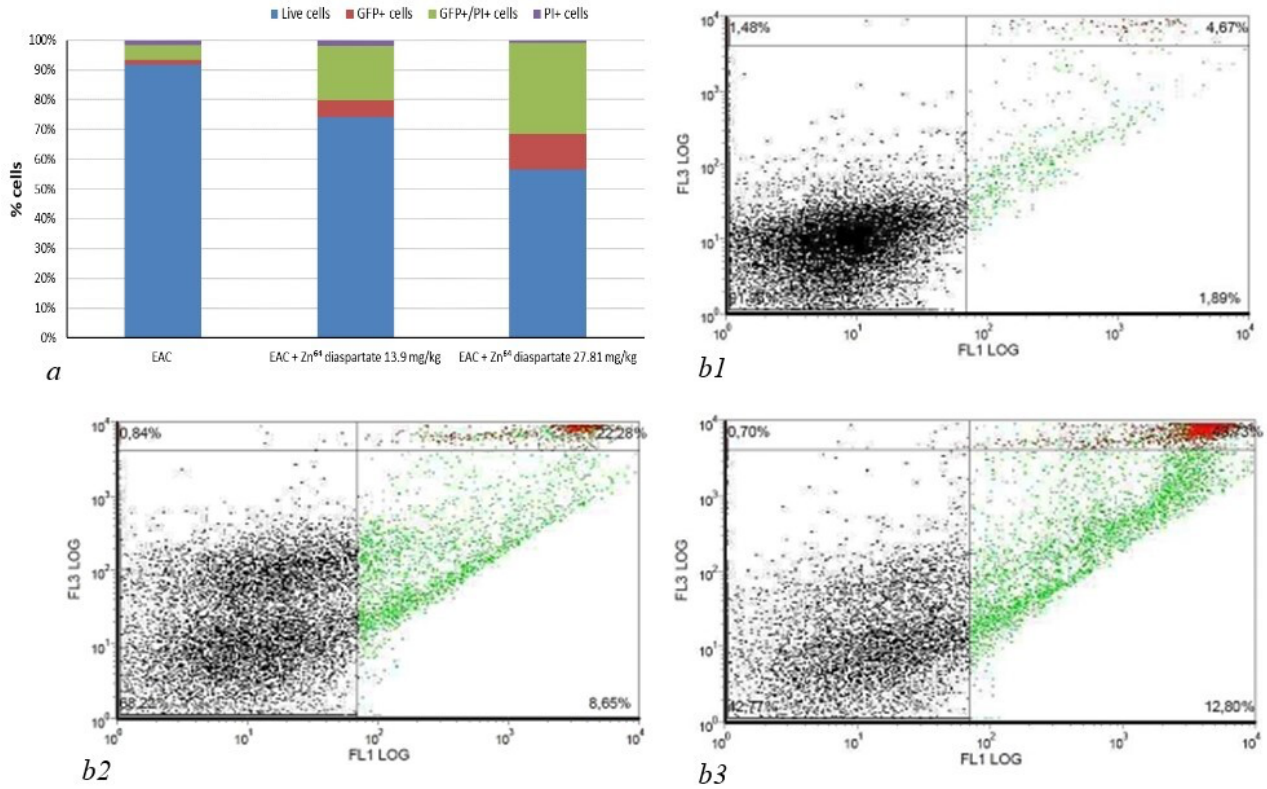


Figure 5. (*a*) Cytometric analysis of apoptotic death of EAC cells treated with Zn^{64} diaspartate. (*b*) Scatter diagrams of EAC cells distributed depending on the PI and GFP fluorescence presence and intensity (n=9). PI^{-}/GFP^{-} - live cells, PI^{+} - dead cells, PI^{+}/GFP^{+} - late stage apoptosis cells, GFP^{+} – early/middle stage apoptosis cells. (*b1*) – EAC, (*b2*) - EAC + Zn^{64} diaspartate 13.9 mg/kg, (*b3*) - EAC + Zn^{64} diaspartate 27.81 mg/kg.

Twenty-four hours after Zn^{64} diaspartate administration, EAC cells showed a 1.4- to 1.9-fold increase in ROS production, compared to control (Figure 6). Zinc is generally redox-inert, so zinc compounds typically raise ROS indirectly by perturbing redox homeostasis (mitochondria, NADPH oxidases, thiol chemistry), rather than via a Fenton-like ROS generation. Reviews on zinc/redox homeostasis emphasize this “indirect control” via sulfur/thiol binding and zinc release/redistribution [17]. The detected increase in ROS levels is “small” in absolute terms, but in cancer biology it can still be mechanistically meaningful because many malignant cells already sit close to a redox threshold [18]. If baseline ROS levels are already elevated, a ~1.5× increase can be sufficient to trigger p53 stress responses and intrinsic apoptosis [19]. A modest elevation in labile intracellular zinc may be sufficient to alter signaling and cell-fate programs, in particular

apoptosis, without inducing a massive oxidative burst. The “indirect control” via sulfur/thiol binding preferentially binds isotopically light ^{64}Zn due to coordination chemistry.

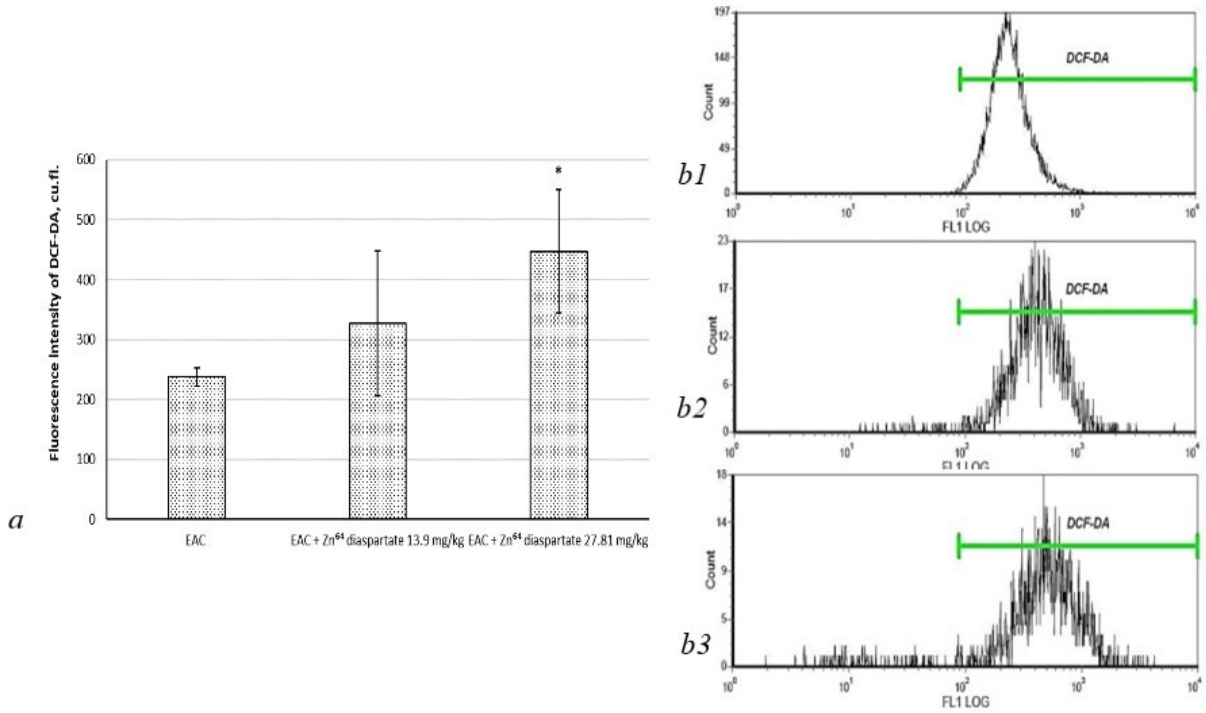


Figure 6. (*a*) Effects of Zn^{64} diaspartate on the production of ROS in EAC cells. (*b*) Fluorescence intensity of DCF-DA in Zn^{64} diaspartate-treated EAC cells (n=6). (*b1*) – EAC, (*b2*) – EAC + Zn^{64} diaspartate at the dose of 13.9 mg/kg, (*b3*) – EAC + Zn^{64} diaspartate at the dose of 27.81 mg/kg. *The difference between treated and control groups is statistically significant when $p<0.05$

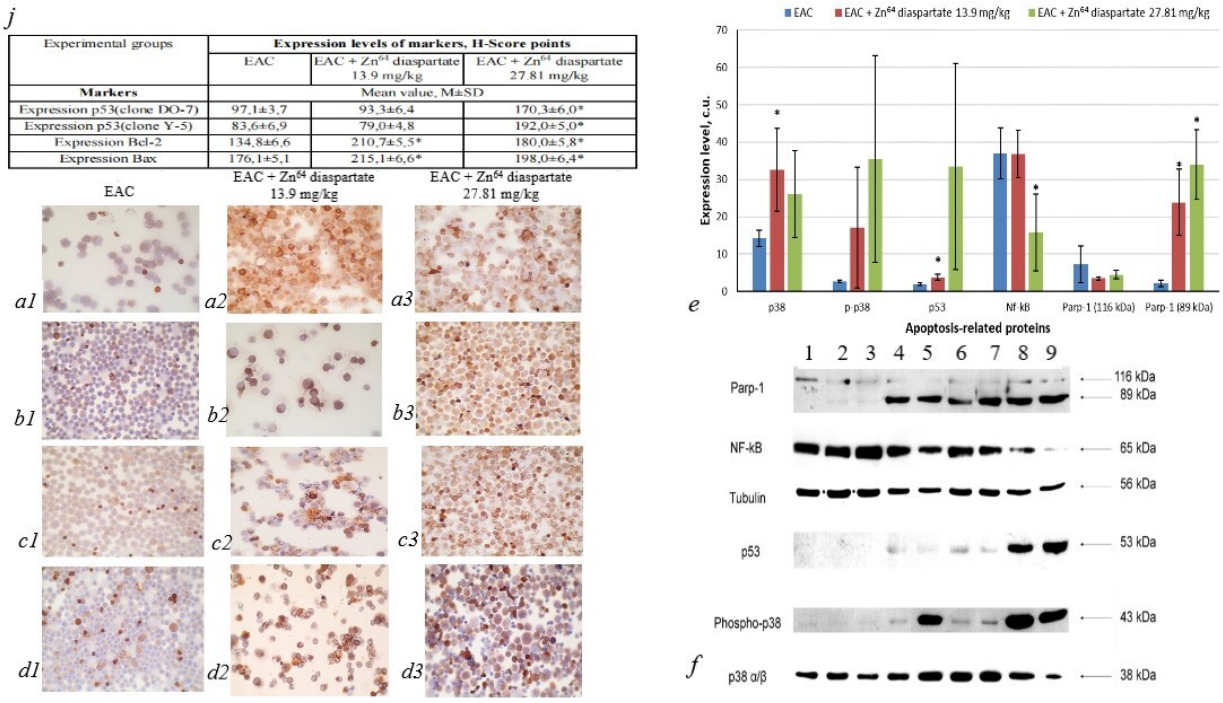


Figure 7. Effect of Zn^{64} diaspartate on the expression of apoptosis-regulating proteins in EAC cells. (*j*) Results of immunocytochemical analysis of the pro- and anti-apoptotic proteins expression in EAC cells treated with Zn^{64} diaspartate (n=9). (*a-d*) Photo of EAC cells after immunohistochemical staining: (*a1-a3*) - Bcl-2 expression, (*b1-b3*) - Bax expression, (*c1-c3*) - p53 expression (clone Y-5), (*d1-d3*) - p53 expression (clone DO-7), magnification x400. (*e*) Results of Western blot analysis (densitometry) of apoptosis-related proteins expression in Zn^{64} diaspartate-treated EAC cells (n=3). (f) Blotogram the quantity of apoptosis-related proteins expression in EAC cells treated with Zn^{64} diaspartate. (1-3) – EAC, (4-6) – EAC + Zn^{64} diaspartate at the dose of 13.9 mg/kg, (7-9) – EAC + Zn^{64} diaspartate at the dose of 27.81 mg/kg. *The difference between experimental and control groups is statistically significant when $p<0.05$.

Literature reports that ROS can induce p38 phosphorylation in BC cells, which is accompanied by suppression of proliferation and activation of apoptosis in tumor cells [20]. The results of Western blot analysis indicate an increased expression of p38 MAPK α/β isoforms in both inactive (p38) and active (p-p38) forms (Figure 7e, 7f). In this case, the p-p38/p38 ratio in the animal groups treated with Zn^{64} diaspartate increased by 2.3–8.6-fold relative to control, which may indicate antiproliferative and proapoptotic effects of Zn^{64} diaspartate in BC. Conclusively, in EAC cells, Zn^{64} diaspartate induced activation of p38 MAPK via ROS.

The transcription factor NF-κB is another important apoptosis-regulating protein in tumor cells, whose activity can be influenced by the intracellular ROS level [21]. The results of Western blot analysis show that in EAC cells treated with Zn^{64} diaspartate, NF-κB expression decreased by 57% compared to control (Figure 7e, 7f). NF-κB is considered an antiapoptotic factor, and its

increased level can activate the expression of other antiapoptotic proteins and antioxidant enzymes [22]. Therefore, a decrease in NF-κB levels can induce and enhance apoptosis of tumor cells [23, 24]. The additional consideration is that not only the increase in ROS, but also the changes we observed in p-p38/p38 expression may explain the effect of Zn^{64} diaspartate on NF-κB levels in carcinoma cells. In malignant cells, the p38 MAPK and NF-κB pathways are key signaling cascades, where p38 exerts a negative regulatory effect on NF-κB activation through a feedback mechanism [25], which can also trigger apoptosis and suppress the proliferation of BC cells [26].

Activation of p38 leads to phosphorylation of multiple transcriptional regulators that coordinate proliferation, the cell cycle, and the apoptotic program in malignant cells. In particular, p-p38 can enhance cytoplasmic expression of the proapoptotic protein p53 by stabilizing it [27]. Accumulation of p53 in the cytoplasm of cells leads to activation of apoptosis via the intrinsic, mitochondria-mediated pathway, which is characterized by permeabilization of the outer mitochondrial membrane and results in programmed cell death [28]. Immunohistochemical analysis in this study demonstrated a statistically significant, approximately twofold increase in cytoplasmic p53 expression in EAC cells after Zn^{64} diaspartate injection compared with the control group (Figure 7j, 7c, 7d). An increase in this parameter in lysates of carcinoma cells treated with Zn^{64} diaspartate was also confirmed by Western blot analysis (Figure 7e, 7f). Furthermore, p53 is also a target for ROS and is susceptible to redox modification at cysteine or tyrosine residues. Such biochemical modifications of p53 can alter its conformation and subcellular localization, thereby affecting the stability, DNA binding, transcriptional activity, and biological functions of the protein [29]. Thus, ROS induce activation of p53 and its translocation to mitochondria, where p53 acts as a direct activator of Bax [30]. In this study, Zn^{64} diaspartate performed a similar function, since isotopically light zinc ions preferentially coordinate with cysteine residues, helping to maintain the wild-type structure of p53 protein and modifying its functional activity [31]. In this context, taking into account the effect of equilibrium isotope fractionation, where lighter isotopes are enriched in bonds with lower bond energy [31], Zn^{64} diaspartate may be more active than zinc with the natural isotopic distribution.

Results of immunocytochemical analysis indicate a statistically significant increase in cytoplasmic expression of the proapoptotic protein Bax in EAC cells after Zn^{64} diaspartate injection by 12 – 22% compared to the control group (Figure 7j, 7b). Activation of Bax as a result of its interaction with p53 leads to translocation of this protein to mitochondria and its oligomerization, which is accompanied by pore formation in the outer mitochondrial membrane and release of cytochrome C from the inner membrane compartment of the organelles [32].

As a marker of impaired mitochondrial function and cytochrome C release in EAC cells after Zn^{64} diaspartate injection, we used biochemical characteristics of cardiolipin status. Analysis

of biochemical changes in mitochondrial cardiolipin in EAC cells treated with Zn^{64} diaspartate showed cardiolipin peroxidation as evidenced by a statistically significant decrease in the NAO fluorescence intensity ratio by 50.3% compared to the control group (Figure 8). This leads to changes in its conformation, phospholipid translocates to the outer mitochondrial membrane and contributes to the formation of a pore through which cytochrome C can be released. The release of cytochrome C from the mitochondrial intermembrane space into the cytosol triggers downstream apoptotic events [33].

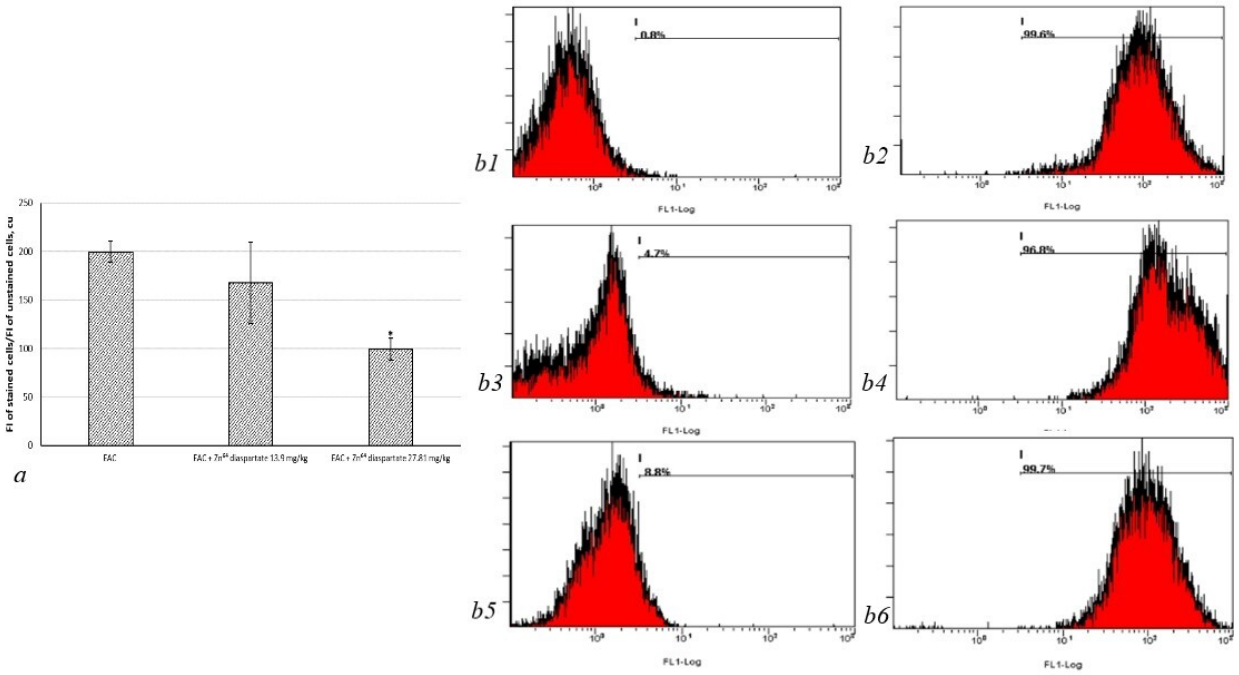


Figure 8. (a) Analysis of the biochemical changes of mitochondrial cardiolipin in EAC cells treated with Zn^{64} diaspartate *in vivo* (n=6). (*b*) Histograms of NAO fluorescence intensity in EAC cells treated with Zn^{64} diaspartate *in vivo*. (*b1*) – EAC unstained cells, (*b2*) – EAC NAO-stained cells, (*b3*) - EAC + Zn^{64} diaspartate at the dose of 13.9 mg/kg unstained cells, (*b4*) – EAC + Zn^{64} diaspartate at the dose of 13.9 mg/kg NAO-stained cells, (*b5*) - EAC + Zn^{64} diaspartate at the dose of 27.81 mg/kg unstained cells, (*b6*) - EAC + Zn^{64} diaspartate at the dose of 27.81 mg/kg NAO-stained cells. *The difference between experimental and control groups is statistically significant when $p<0.05$.

The most compelling evidence of apoptosis activation in carcinoma cells treated with Zn^{64} diaspartate was a marked increase in the cleaved form of PARP-1 (poly(ADP-ribose) polymerase) with a molecular weight of 89 kDa. Western blot analysis of EAC cell lysates after a single administration of Zn^{64} diaspartate showed an 11–16-fold increase in fragmented PARP-1 compared to control (Figure 7e, 7f). Moreover, according to our Annexin V/PI viability assay,

treatment with Zn^{64} diaspartate led to the increase in the proportion of tumor cells, predominantly in the late phase of apoptosis. At this stage, mitochondrial functional activity was impaired and caspases, particularly caspase-9 and caspase-3, were activated. Caspase-3 in turn cleaves PARP-1, resulting in accumulation of fragmented PARP-1 in the cells, which serves as an informative marker of apoptosis in EAC cells.

We also observed a statistically significant increase in the expression of the antiapoptotic protein Bcl-2 by 33.5-56.3% in EAC cells after Zn^{64} diaspartate injection (Figure 7j, 7a). Plausibly, we hypothesized that this is a compensatory mechanism used by the survived carcinoma cells in reaction to a single administration of Zn^{64} diaspartate. Given the apoptosis activation mechanism and antitumor efficacy of Zn^{64} diaspartate established by us *in vivo*, and relying on literature data indicating that p53 can sequester Bcl-2 through direct physical interaction [34], a continuous treatment with Zn^{64} diaspartate may provide cytotoxic concentrations sufficient to induce irreversible commitment of EAC cells to apoptosis.

Thus, our results indicate that Zn^{64} diaspartate inhibits EAC growth in a dose-dependent manner and induces tumor cell death via activation of the intrinsic, mitochondria-mediated ROS/p53-dependent apoptotic pathway.

Funding information:

The research was funded by the Vector Vitale LLC, North Miami Beach, FL 33160, USA.

Data Availability:

The data that support the findings of this study are available from the corresponding author, [Sergey Gurin, s.v.gurin@gmail.com], upon reasonable request.

References

1. Menon G, Alkabban FM, Ferguson T. Breast Cancer. 2024. In: StatPearls [Internet]. Treasure Island (FL): StatPearls Publishing; 2026 Jan–.
2. Pan Z, Choi S, Ouadid-Ahidouch H, Yang JM, Beattie JH, Korichneva I. Zinc transporters and dysregulated channels in cancers. Front Biosci (Landmark Ed). 2017;22(4):623-643.
3. Gialeli C, Theocharis AD, Karamanos NK. Roles of matrix metalloproteinases in cancer progression and their pharmacological targeting. FEBS J. 2011;278(1):16-27.
4. Kelleher SL, Seo YA, Lopez V. Mammary gland zinc metabolism: regulation and dysregulation. Genes Nutr. 2009;4(2):83-94.
5. Sullivan KV, Moore RET, Capper MS, Schilling K, Goddard K, Ion C, Layton-Matthews D, Leybourne MI, Coles B, Kreissig K, Antsygina O, Coombes RC, Larner F, Rehkämper

M. Zinc stable isotope analysis reveals Zn dyshomeostasis in benign tumours, breast cancer, and adjacent histologically normal tissue. Metallomics. 2021;13(6):mfab027.

6. Larner F, Woodley LN, Shousha S, Moyes A, Humphreys-Williams E, Strekopytov S, Halliday AN, Rehkämper M, Coombes RC. Zinc isotopic compositions of breast cancer tissue. Metallomics. 2015;7(1):112-7.
7. Chen B, Yu P, Chan WN, Xie F, Zhang Y, Liang L, Leung KT, Lo KW, Yu J, Tse GMK, Kang W, To KF. Cellular zinc metabolism and zinc signaling: from biological functions to diseases and therapeutic targets. Signal Transduct Target Ther. 2024;9(1):6.
8. Franklin RB, Costello LC. The important role of the apoptotic effects of zinc in the development of cancers. J Cell Biochem. 2009;106(5):750-7.
9. Radulski DR, Stipp MC, Galindo CM, Acco A. Features and applications of Ehrlich tumor model in cancer studies: a literature review. Transl Breast Cancer Res. 2023;4:22.
10. Watkins EJ. Overview of breast cancer. JAAPA. 2019;32(10):13-17.
11. Krezoski SK, Villalobos J, Shaw CF 3rd, Petering DH. Kinetic lability of zinc bound to metallothionein in Ehrlich cells. Biochem J. 1988;255(2):483-91.
12. Novak P, Balakin A, Temnik M. *In Vitro* Anticancer Activity of the Light Stable Zinc Isotope (^{64}Zn) Compounds. Anticancer Res. 2022;42(12):5685-5698.
13. Osman AM, Alqahtani AA, Damanhouri ZA, Al-Harthy SE, ElShal MF, Ramadan WS, Kamel F, Osman MA, Khan LM. Dimethylsulfoxide excerbates cisplatin-induced cytotoxicity in Ehrlich ascites carcinoma cells. Cancer Cell Int. 2015;15:104.
14. Hashemi M, Khosroshahi EM, Chegini MK, Asadi S, Hamyani Z, Jafari YA, Rezaei F, Eskadehi RK, Kojoori KK, Jamshidian F, Nabavi N, Alimohammadi M, Rashidi M, Mahmoodieh B, Khorrami R, Taheriazam A, Entezari M. Mechanistic insights into cisplatin response in breast tumors: Molecular determinants and drug/nanotechnology-based therapeutic opportunities. Mutat Res Rev Mutat Res. 2024;794:108513.
15. Kocyła A, Adamczyk J, Krężel A. Interdependence of free zinc changes and protein complex assembly - insights into zinc signal regulation. Metallomics. 2018;10(1):120-131.
16. Fu YC, Liang SB, Luo M, Wang XP. Intratumoral heterogeneity and drug resistance in cancer. Cancer Cell Int. 2025;25(1):103.
17. Oteiza PI. Zinc and the modulation of redox homeostasis. Free Radic Biol Med. 2012;53(9):1748-59.
18. Trachootham D, Alexandre J, Huang P. Targeting cancer cells by ROS-mediated mechanisms: a radical therapeutic approach? Nat Rev Drug Discov. 2009;8(7):579-91.

19. Provinciali M, Pierpaoli E, Bartozzi B, Bernardini G. Zinc Induces Apoptosis of Human Melanoma Cells, Increasing Reactive Oxygen Species, p53 and FAS Ligand. Anticancer Res. 2015;35(10):5309-16.
20. Woo CC, Hsu A, Kumar AP, Sethi G, Tan KH. Thymoquinone inhibits tumor growth and induces apoptosis in a breast cancer xenograft mouse model: the role of p38 MAPK and ROS. PLoS One. 2013;8(10):e75356.
21. Lingappan K. NF-κB in Oxidative Stress. Curr Opin Toxicol. 2018;7:81-86.
22. Wu X, Sun L, Xu F. NF-κB in Cell Deaths, Therapeutic Resistance and Nanotherapy of Tumors: Recent Advances. Pharmaceuticals (Basel). 2023;16(6):783.
23. Hernandez L, Kim MK, Noonan AM, Sagher E, Kohlhammer H, Wright G, Lyle LT, Steeg PS, Anver M, Bowtell DD; Australian Ovarian Cancer Study Group 57; Annunziata CM. A dual role for Caspase8 and NF-*κ*B interactions in regulating apoptosis and necroptosis of ovarian cancer, with correlation to patient survival. Cell Death Discov. 2015;1:15053.
24. Hao S, Li S, Wang J, Zhao L, Yan Y, Wu T, Zhang J, Wang C. C-Phycocyanin Suppresses the In Vitro Proliferation and Migration of Non-Small-Cell Lung Cancer Cells through Reduction of RIPK1/NF-κB Activity. Mar Drugs. 2019;17(6):362.
25. Dong X, Li JC, Jiang YY, Xia MY, Tashiro S, Onodera S, Ikejima T. p38-NF-κB-promoted mitochondria-associated apoptosis and G2/M cell cycle arrest in norcantharidin-treated HeLa cells. J Asian Nat Prod Res. 2012;14(11):1008-19.
26. Hong B, Li H, Zhang M, Xu J, Lu Y, Zheng Y, Qian J, Chang JT, Yang J, Yi Q. p38 MAPK inhibits breast cancer metastasis through regulation of stromal expansion. Int J Cancer. 2015;136(1):34-43.
27. Yue J, López JM. Understanding MAPK Signaling Pathways in Apoptosis. Int J Mol Sci. 2020;21(7):2346.
28. Mihara M, Erster S, Zaika A, Petrenko O, Chittenden T, Pancoska P, Moll UM. p53 has a direct apoptogenic role at the mitochondria. Mol Cell. 2003;11(3):577-90.
29. Maillet A, Pervaiz S. Redox regulation of p53, redox effectors regulated by p53: a subtle balance. Antioxid Redox Signal. 2012;16(11):1285-94.
30. Chipuk JE, Kuwana T, Bouchier-Hayes L, Droin NM, Newmeyer DD, Schuler M, Green DR. Direct activation of Bax by p53 mediates mitochondrial membrane permeabilization and apoptosis. Science. 2004;303(5660):1010-4.
31. Balter V, Lamboux A, Zazzo A, Télouk P, Leverrier Y, Marvel J, Moloney AP, Monahan FJ, Schmidt O, Albarède F. Contrasting Cu, Fe, and Zn isotopic patterns in organs and body fluids of mice and sheep, with emphasis on cellular fractionation. Metallomics. 2013;5(11):1470-82.

32. Chipuk JE, Green DR. Cytoplasmic p53: bax and forward. Cell Cycle. 2004;3(4):429-31.
33. Asumendi A, Morales MC, Alvarez A, Aréchaga J, Pérez-Yarza G. Implication of mitochondria-derived ROS and cardiolipin peroxidation in N-(4-hydroxyphenyl)retinamide-induced apoptosis. Br J Cancer. 2002;86(12):1951-6.
34. Wei H, Wang H, Wang G, Qu L, Jiang L, Dai S, Chen X, Zhang Y, Chen Z, Li Y, Guo M, Chen Y. Structures of p53/BCL-2 complex suggest a mechanism for p53 to antagonize BCL-2 activity. Nat Commun. 2023;14(1):4300.